Changes in the Elastic Properties of Cholinergic Synaptic Vesicles as Measured by Atomic Force Microscopy

Daniel E. Laney,* Ricardo A. Garcia,# Stanley M. Parsons,# and Helen G. Hansma*

*Department of Physics, University of California, Santa Barbara, California 93106, and #Department of Chemistry, Biochemistry and Molecular Biology Program, and the Neuroscience Research Institute, University of California, Santa Barbara, California 93106 USA

ABSTRACT Cholinergic synaptic vesicles from *Torpedo californica* have been probed with the atomic force microscope in aqueous buffers to map and measure their elastic properties. Elastic properties were mapped with a new atomic force microscope technique known as force mapping. Force mapping of vesicles showed that the centers of the vesicles are harder or stiffer than the peripheral areas in the three buffers that were investigated. These were an isoosmotic buffer, a hypoosmotic buffer, and an isoosmotic buffer with 5 mM $CaCl_2$ added. The hardness of the vesicular centers was quantified by calculation of the elastic modulus. Elastic moduli were in the range of 2–13 $\times$ 10^5 Pa. Vesicular centers were hardest in calcium-containing buffer and softest in isoosmotic buffer. Hypotheses are presented for the composition and function of the hard centers.

INTRODUCTION

The atomic force microscope (AFM) is becoming an increasingly useful research tool in biology (Hansma and Hoh, 1994; Bustamante and Rivetti, 1996; Hansma, 1996; Shao et al., 1996) and neurobiology (Schroff et al., 1995; Miklossy et al., 1994; Henderson et al., 1992). One of the strengths of atomic force microscopy (AFM) is its ability to image in physiological buffers structures as small as DNA, proteins, and pores in arrays of membrane protein channels when these biomaterials are located upon flat surfaces (Radmacher et al., 1994b; Schabert et al., 1995; Hansma et al., 1995). The AFM images sample surfaces by raster scanning a sharp tip across the sample surface. The tip is on the end of a cantilever, which responds to angstrom-sized changes in the heights of surface features.

The AFM also can give information about the material properties of biological samples. One way to obtain such information is with AFM force plots, in which the AFM tip moves up and down over a point on the sample surface, probing the elastic and adhesive properties of materials such as rubber, polyurethane, gelatin, living cells, and microtubules (Tau et al., 1992; Weisenhorn et al., 1993; Radmacher et al., 1995; Vinckier et al., 1996). A natural extension of AFM force plots is the acquisition of complete maps of the material properties of the sample. This technique, called force mapping, has been used to study the surface properties of substrates such as molecules of the enzyme lysozyme, DNA, and human platelets (Radmacher et al., 1994a, 1996). In this study we have force mapped cholinergic synaptic vesicles from the electric organ of *Torpedo californica*, a marine ray. These vesicles release the neurotransmitter acetyl choline into the synaptic cleft, where it triggers an action potential in the postsynaptic cell.

Many of the molecular mechanisms that govern vesicle exocytosis are conserved from yeast to mammalian brain (Calakos and Scheller, 1996). Thus, further studies of a well-characterized system such as *Torpedo* may provide insights that can eventually be applied to larger problems, such as Alzheimer's disease, which is characterized by a loss of cholinergic synapses (Marx, 1996). The biomechanical properties of synaptic vesicles must play a role in the exocytosis and subsequent recycling of the vesicles. The AFM has already been used to visualize synaptic vesicles in fluid environments and to observe changes in vesicle size and shape (Parpura et al., 1995). With AFM force mapping we show here both a substructure in cholinergic synaptic vesicles and also buffer-dependent changes in vesicular elasticity.

MATERIALS AND METHODS

Materials

VP1 reserve synaptic vesicles were purified from the electric organ of *Torpedo californica* (Noremberg and Parsons, 1989; Gracz and Parsons, 1996). The isolation involves homogenization of electric organs, differential velocity sedimentation, neutral buoyancy banding, and size exclusion chromatography of vesicles. Approximately 95% pure vesicles of ~108-nm diameter are obtained at a final concentration of 10–100 μg of protein/mL in isoosmotic buffer composed of 820 mM glycine, 5 mM HEPES, 1 mM EDTA, 1 mM EGTA, 3 mM NaN_3, and 2 μM butylated hydroxy toluene adjusted to pH 7.0 with KOH. All chemicals were obtained from usual commercial sources and were of reagent or better grade.

Instrumentation

All data were gathered on a Nanoscope III with a MultiMode AFM (Digital Instruments, Santa Barbara, CA). Force maps were captured by a β-test release of the Nanoscope III software version 4.1. Use of this software did not require external electronics. Force maps were captured with 200-μm-long "narrow" V-shaped oxide-sharpened cantilevers (Nanoprobe, Digital Instruments, Santa Barbara, CA). All cantilevers were imaged in a scan-

ning electron microscope before use so that the radii of curvature of the tips could be estimated. The spring constants of the cantilevers were measured by the thermal noise method (Hutter and Bechhoefer, 1993; Walters et al., 1996) and were typically $\sim$0.04 N/m.

AFM operation

Disks of ruby mica (S and J Trading Company, Glen Oaks, NY) were glued to steel disks with 2-Ton epoxy (Devcon Corp., Wood Dale, IL) and cleaved with Scotch tape (3 M Corp., Minneapolis, MN). A freshly cleaved mica disk was placed in the AFM. Forty microliters of vesicle suspension was deposited onto the cantilever in the fluid cell. The fluid cell was placed into the AFM, which brought the vesicle suspension into contact with the mica surface.

Force maps were captured in three buffer environments: isoosmotic buffer, hypoosmotic buffer, and isoosmotic buffer with 5 mM $CaCl_2$ (calcium buffer). Samples were equilibrated to room temperature for $\sim$5 min before engaging.

Isoosmotic buffer and calcium buffer had 10–20 mM $MgCl_2$ added to facilitate the binding of the vesicles to the mica surface. Force maps in hypoosmotic buffer were captured as follows: First, vesicles in isoosmotic buffer were placed in the microscope as described above. Second, MilliQ water (Burlington, MA) was added until the final buffer composition was 60% isoosmotic buffer and 40% water. The water was added in situ by use of a syringe with a thin ceramic needle (World Precision Instruments, Sarasota, FL) guided by a specially designed fluid injection port. We estimated the length of time required for mixing in a separate experiment by adding dye to the fluid cell and waiting for it to diffuse. Images were taken 5 min or more after the addition of water, which was sufficient time for the vesicles to adapt to the hypoosmotic environment. We calibrated cantilever deflection in nanometers by measuring the sensitivity of the cantilever before each experiment, using the Nanoscope software.

Force mapping software

The force mapping software takes a force plot at each point in a two-dimensional scan of the sample. The software allows the user to choose the number of data points per force plot and the number of force plots per scan line. A trade-off must be made between these two parameters, because the software limits the size of the data sets.

Force maps were captured in "relative triggering mode." Using this mode ensures that the maximum cantilever deflection caused by the sample is the same in every force plot. In this mode the user selects the vertical (Z-) scan distance and the maximum cantilever deflection. In these experiments the Z-scan distance was 32 nm and the maximum cantilever deflection was 7 nm. For each force plot, first the deflection is recorded when the tip and the sample are apart, and this value is used to calculate changes in deflection. Then the sample is pressed into the tip until the cantilever deflection has increased by the maximum deflection amount (the upper, "extend" plot; Fig. 1 A). The sample is then retracted by an amount equal to the Z-scan size (the lower, "retract" plot; Fig. 1 A). The whole process is repeated for each point in the X–Y scan. The actual start and end positions of the sample in each force plot depend on the height and the elasticity of the surface features. This mode is useful because it compensates for the thermal drift of the cantilever deflection before each force plot is acquired.

Force plots with discontinuities in deflection are discarded. If the Z-scan size is comparable with the height of the vesicle it is safest to discard the force plots on the left side of the vesicle in the case of a left-to-right fast scan direction. This is so because the abrupt change in height between the mica and the vesicle permits a side interaction that can cause the tip to remain in contact with the vesicle after the retract part of a force plot. Larger Z-scan sizes eliminate this artifact but at the cost of lower resolution in the Z position of the sample.

Force maps of vesicles were composed of 64 × 64 force plots sampled at 64 points each per extend and retract force plots. The X–Y-scan size was 1000 nm, and the Z-scan distance was 32 nm. The scan angle was 0°,
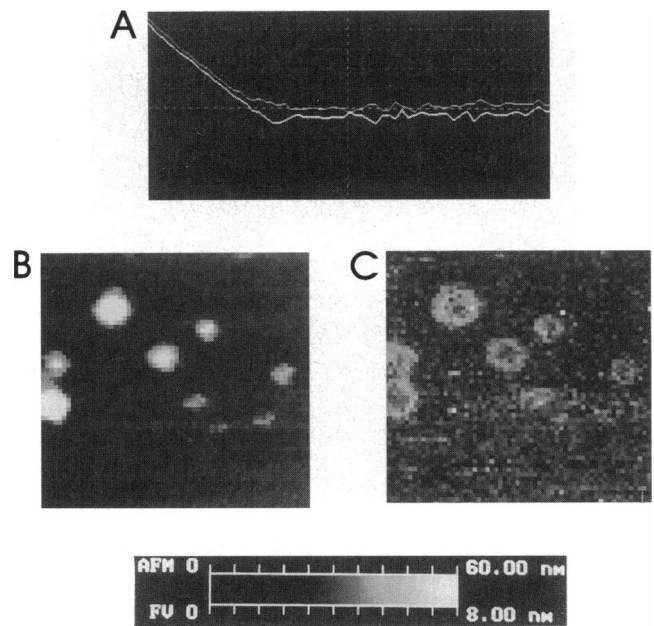

FIGURE 1   Data displayed by the force mapping software. A, Force plot on mica, showing extend (*upper*) and retract (*lower*) curves. Vertical axis, cantilever deflection, 16-nm full scale; horizontal axis, sample position in the vertical (Z) direction, 32-nm full scale. The force at any deflection can be found by multiplying the cantilever deflection by the spring constant of the cantilever. B, The height image of synaptic vesicles in isoosmotic buffer, showing surface topography. C, The FV image of the same synaptic vesicles, showing cantilever deflection from the retract force plots at a Z position $\sim$16 nm from the point of maximum applied force. At Z = 0 nm (sample at maximum applied force) and Z = 32 nm (cantilever off the surface) this image is featureless. The gray scale at the bottom correlates with the AFM height image and the deflection range of the FV image. Images in B and C are 1 μm × 1 μm.

corresponding to a fast scan direction parallel to the long axis of the cantilever. A Z-scan speed of 9.77 Hz was used to capture force maps, giving an X–Y-scan speed of 0.07 Hz (one line every 14–15 s). This speed permitted the capture of a complete force map in 15 min with reasonable lateral resolution and without the problems of hydrodynamic drag that are seen with faster Z-scan speeds (Radmacher et al., 1996).

A family of force volume images can be plotted from each force map. A force volume image (e.g., Fig. 1 C) is a map of the cantilever deflection at each point on the sample surface at a constant Z position of the sample.

Tip radii

The tip radii were used in calculating the elastic modulus of vesicles. Tip radii were estimated from scanning electron micrographs at 100,000× (Fig. 2). Electron micrographs were scanned and imported into a paint program. We drew circles in the ends of the tips to estimate the tip radii, which were typically 11–23 nm.

Calculating elastic properties

The Hertz model (Weisenhorn et al., 1993; Radmacher et al., 1995) was used to model the elastic response of synaptic vesicles indented by an infinitely hard spherical AFM tip. Modeling the tip and the vesicle as spheres is appropriate because the radii of the tip and the vesicles are comparable. The model is useful as long as the indentations involved are smaller than the radius of curvature of the tip. Roark (Young, 1989) gives
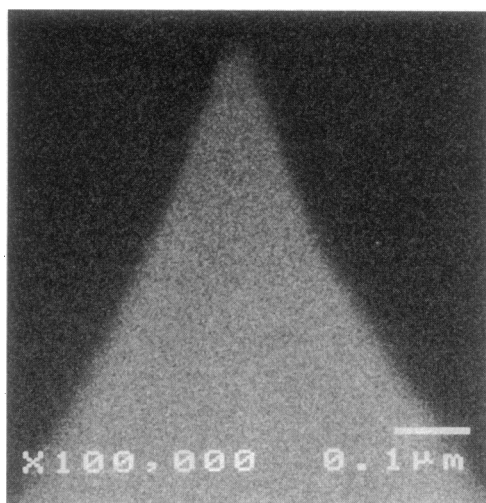
FIGURE 2 Scanning electron micrograph of typical AFM tip used to image vesicles.

the following formula for the indentation δ for this model:

$$\delta = 1.04\left[\frac{F^2(D_{tip} + D_{ves})\left(\dfrac{1 - \nu_{tip}^2}{E_{tip}} + \dfrac{1 - \nu_{ves}^2}{E_{ves}}\right)^2}{D_{tip}D_{ves}}\right]^{1/3}, \quad (1)$$

where F is the applied force, E is the elastic modulus (or Young's modulus), D is the diameter, and ν is Poisson's ratio. The properties associated with the tip and the vesicle are denoted by subscripts.

Letting $D_{tip,\ ves} = 2R_{tip,\ ves}$ and $E_{tip} = \infty$ gives

$$\delta = 0.825\left[\frac{F^2(1 - \nu_{ves}^2)^2(R_{tip} + R_{ves})}{E_{ves}^2 R_{tip} R_{ves}}\right]^{1/3}. \quad (2)$$

For an AFM tip in contact with a hard surface, a change in the Z position causes an equal change in the cantilever deflection. On a soft sample, the tip also indents into the soft surface. Thus the change in Z position is the sum of the change in deflection plus the indentation:

$$z - z_0 = d - d_0 + \delta, \quad (3)$$

where z is the Z position, z_0 is the contact point, d is the deflection, and d_0 is the noncontact deflection. Letting $F = k(d - d_0)$ in Eq. 2, where k is the spring constant of the cantilever, and substituting Eq. 2 into Eq. 3 yield

$$z - z_0 \quad (4)$$
$$= d - d_0 + 0.825\left[\frac{k^2(1 - \nu_{ves}^2)^2(R_{tip} + R_{ves})}{E_{ves}^2 R_{tip} R_{ves}}\right]^{1/3} (d - d_0)^{2/3}.$$

Data from force mapping were exported to IGOR Pro (Wavemetrics, Lake Oswego, OR) data analysis software. Fig. 3 A shows how indentation was estimated. The resulting error is typically ±1.0 nm for indentations of ~10 nm.

The following procedure was used to calculate elastic modulus from force plots: The extend and retract plots were averaged. The value for d_0 was taken to be the average of several points at the right-hand end of the force plot. It was often difficult to identify precisely the contact point (z_0) from the force plots (see, e.g., Fig. 1 A). Therefore, Eq. 4 was fitted to the values for z and d, with E and z_0 used as the fit parameters (Fig. 3 B). The noncontact regime was not used in the fit. The equation was not fitted to data for which the indentation was more than 10 nm or the tip radius
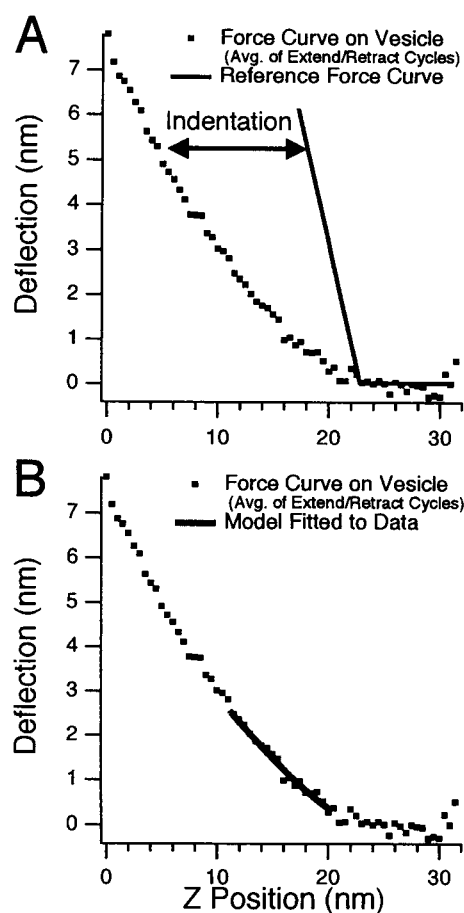

FIGURE 3 Extracting indentation (A) and elastic modulus (B) from a force plot on a vesicle. The extend–retract plots have been averaged. A, Indentation is calculated by finding the difference in Z position between a force plot on a vesicle and a force plot on mica at a specified deflection. The mica and vesicle force plots have been offset so that the contact points coincide. The slope of the reference force plot on mica is calculated by averaging the slopes of the contact portions of many force plots on bare mica areas of the FV image. Uncertainty in the contact point results in an error of ±1 nm for the estimated indentation. B, The result of fitting the function $z = z_0 + d - d_0 + A(d - d_0)^{(2/3)}$ to the data in the curvature region, where z is the Z position, z_0 is the contact point, d is the deflection, and d_0 is the noncontact deflection. The free parameters were z_0 and A. The elastic modulus was then extracted from A according to Eq. 4 with Poisson's ratio set to 0.5. Tip radii were estimated from electron micrographs. Vesicle diameter was estimated from the vesicle height after it was corrected for indentation.

(whichever was smaller). The cutoff value of 10 nm was selected because it is typically less than 25% of vesicle height. The fit was evaluated by two methods. In the first, χ^2 was minimized for each force plot. In the second, the fit was visually examined by the user to ensure that the z_0 returned by the curve fit was consistent with the data. Multiple force plots from each vesicle were analyzed, and the results were averaged. Only force plots from the middles of the vesicles were analyzed with Eq. 4 because the model does not apply to off-center loading forces.

Statistical analysis

The Wilcoxon rank-sum test (Lapin, 1975) was used to test for differences in the elastic moduli of vesicles in different buffers. Statistically significant

differences had $p < 0.01$, where p is the probability that two populations are the same.

RESULTS AND DISCUSSION

Force plots

A typical AFM force plot on a hard surface is shown in Fig. 4 A. A force plot is a force-versus-distance plot for the cantilever moving up and down in the Z direction above the sample. The horizontal axis of the force plot is the Z position of the AFM tip relative to the sample, and the vertical axis is either the force exerted by the tip on the sample or the cantilever deflection. The noncontact region of the force plot is the horizontal part at the right, as can be seen from the cartoon balloons in Fig. 4 A. When the cantilever deflection is plotted, the slope of the contact region ideally is 1.0 for a very hard surface such as mica

because for every 1 nm of sample movement in the vertical direction the cantilever is deflected by 1 nm.

An actual force plot on mica is shown in Fig. 1 A. The upper curve traces the cantilever deflection as the sample is moved toward the cantilever (the "extend" plot, traced right to left). The lower curve traces the cantilever deflection as the sample is moved away from the cantilever (the "retract" plot, traced left to right). The researcher can choose the maximal cantilever deflection allowed (typically 7 nm), after which the sample is moved away from the cantilever. The extend and retract plots can be averaged to correct for their small vertical separation, which is caused by the movement of the sample in the fluid environment (Radmacher et al., 1996).

Force plots on soft surfaces show a more gradual cantilever deflection because the tip indents the sample (Fig. 4 B). One can estimate the amount of indentation at a particular applied force by aligning the force plots for mica and the soft surface so that the contact points coincide (Figs. 3 A and 4 B).
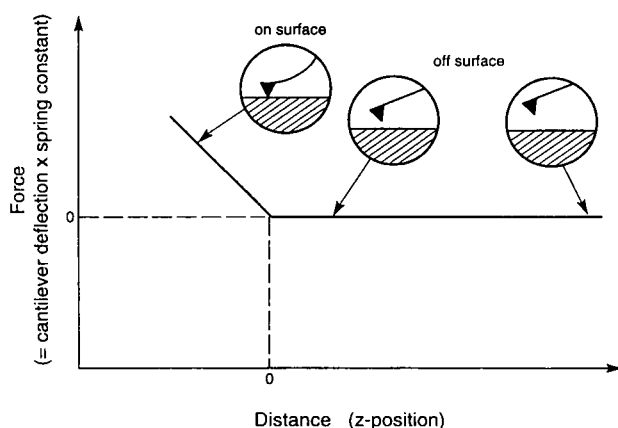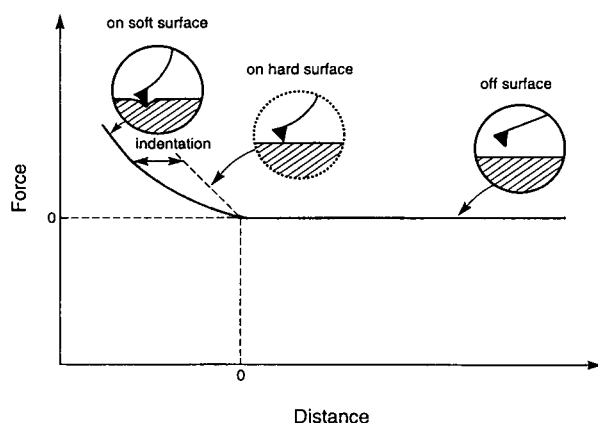
Force mapping

In AFM force mapping a force plot is taken at each point across a sample surface. A height image and a family of force volume (FV) images of the surface can be extracted from the data. A height image for synaptic vesicles in isoosmotic buffer is shown in Fig. 1 B. Three isolated vesicles with apparent diameters of ~90–~150 nm are present. The apparent diameters are larger than the actual diameters by an amount comparable with the diameter of the tip. Diameters of *Torpedo* synaptic vesicles as measured by laser light scattering are 110 ± 25 nm (Gracz and Parsons, 1996).

We obtained the height image in Fig. 1 B by plotting the sample Z position at the maximum allowed cantilever deflection, which yields a topographic map of the sample surface with light areas higher than dark areas. Soft materials such as synaptic vesicles are compressed by the AFM tip; therefore their apparent heights are underestimated. The height image in Fig. 1 B is of relatively low resolution. Low-resolution height images are preferable when one wants to decrease the time required to capture an image and increase the resolution of the force plots by using as much as possible of the available memory per image for data points on the force plots. Tapping mode AFM images at higher resolution gave similar results (R. A. Garcia et al., in preparation).

A FV image is shown in Fig. 1 C for the field of vesicles in Fig. 1 B. This FV image shows variations in softness of the sample surface, on which light regions are softer than dark ones. We constructed the FV image by plotting the deflection of the cantilever at a Z position that was 16 nm away from the position of maximal deflection. This position was chosen because it is in the curvature region of the force plots on vesicles, where the vesicles are undergoing elastic

A

Force Plot on Hard Surface

B

Force Plot on Soft Surface

FIGURE 4   Diagrams of AFM force plots on A, hard and B, soft sample surfaces.

compression. A FV image can be generated at each Z position on the force plot. Other FV images in the curvature region of the force plot are qualitatively similar to those in Fig. 1 C, whereas those at the extremes of maximum cantilever deflection and zero cantilever deflection are almost featureless.

Dark spots of one pixel (16 nm × 16 nm) or more appear in the centers of the vesicles in the FV image of Fig. 1 C. The dark spots, where the cantilever deflections are smaller, are harder than the surrounding lighter-colored, softer regions of the vesicles. The dark spots were present in FV images from both extend and retract force plots of these vesicles at Z-scan speeds of 10–77 Hz. Thus the most likely explanation for the dark spots is that there is an actual structural difference between the centers and the peripheries of the vesicles. The vesicle shapes and positions were unchanged by repeated scanning, which also suggests that the dark centers are not artifacts that are due, for example, to the sliding of the vesicles as their peripheries are probed by the tip.

A typical difference in deflection between the center and the periphery of a vesicle is shown in Fig. 5. The tip–sample contact point is indicated by a zero on the Z-position axis in Figs. 4 and 5. When the force plots are offset so that their contact points coincide, the edge of the vesicle is typically indented approximately twice as much as the center of the vesicle (Fig. 5). The amount that the tip indents the vesicle in Fig. 5 is measured as in Fig. 4 B by comparison with a force plot on mica, which is a hard surface.

Force mapping was done on vesicles in three different buffers, as described in Materials and Methods: a hypoosmotic buffer, an isoosmotic buffer, and a calcium buffer (Fig. 6). All three buffers contained 6–10 mM $MgCl_2$ to facilitate adhesion of the vesicles to the mica surface. The height images of Fig. 6 each show two to four vesicles that appear white because of their relatively large heights. In addition, the height images in hypoosmotic buffer each show one or two flatter (gray-colored) lysed vesicles of variable size. FV images in Fig. 6 correspond to the adjacent height images.

In the FV images, hard centers are seen for vesicles in all three buffers (Fig. 6 A–C). The force plots in Fig. 6 D are a guide to interpreting the FV images in Fig. 6 A–C. The difference in cantilever deflection between the center of the vesicle and the periphery of the vesicle is typically ~1 nm for a Z position of 16 nm, as can be seen from the force plots in Fig. 6 D. These force plots, like the force plots used to generate the images in Fig. 6 A–C, are automatically offset by the AFM software so that the points of maximal deflection coincide. The relative cantilever deflections in Fig. 6 D underestimate the difference in indentation between the center and the periphery of the vesicle because their contact points are at different Z positions. Typical differences in indentation are shown more clearly in Fig. 5, where the contact points of the force plots coincide.

Indentations were estimated over the entire surfaces of several of the vesicles shown in Fig. 6. The indentations were smaller in the center than at the periphery for each vesicle except that in the top FV image of Fig. 6 C with no hard center. For isoosmotic vesicles and calcium vesicles the indentation at the center was 50–70% of the indentation at the edge. Hypoosmotic vesicles showed less difference in indentation across their surfaces, because the indentation at the center was 66–86% of the indentation at the edge.

Elastic moduli

We calculated the elastic moduli (or Young's moduli) for the centers of vesicles in the three buffers by using Eq. 4 from Materials and Methods. The graph of elastic modulus versus vesicle height (Fig. 7) shows that smaller vesicles have larger elastic moduli and thus are generally stiffer or harder. We calculated the vesicle heights in Fig. 7 by adding the height measured from the height image plus the indentation measured from the force plots. There are also buffer-dependent differences in elastic modulus (Fig. 7), as described in the next section.

There are some points to consider when one is interpreting the data. First, the model used to calculate elastic modulus assumes spherical, homogeneous vesicles and a spherical tip. Cholinergic synaptic vesicles are heterogeneous structures at the molecular level, containing a variety of biological macromolecules. Thus, the values obtained for elastic modulus are used for comparison of vesicle popula-
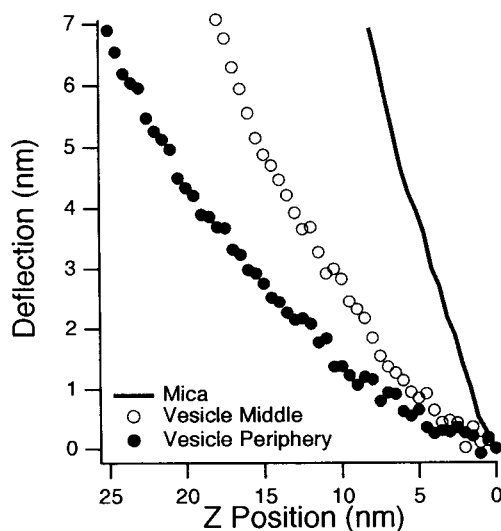

FIGURE 5   Force plots on mica, the middle of a vesicle, and the periphery of a vesicle. The force plots have been offset so that the contact points coincide. The indentation at a given deflection can be estimated from this graph by drawing a horizontal line on it and measuring the difference in Z position between the vesicle plots and the mica plot. In this case the indentation near the periphery of the vesicle is nearly twice as large as that at the center.

FIGURE 6   Corresponding height and FV image images in the following buffers: A, ismotic; B, Ca^{++}-containing; and C, hypoosmotic. Images of two representative fields are shown for each buffer condition. Two to three vesicles can be seen in each height image, which is the topography at the maximum applied force. The FV images show cantilever deflection from the retract force plots at a Z position of 16 nm, where Z = 0 nm corresponds to the sample position at the maximum cantilever deflection. D, The two force plots are a guide to interpreting the FV images. The dashed vertical line shows the Z position at which cantilever deflection is plotted. The arrows point out the difference in deflection between a force plot at the middle of a vesicle and a force plot near the edge of a vesicle. The middle of the vesicle is harder, so there is less Z travel between the contact and the maximum applied force. The result is a longer undeflected portion of the force plot and noncoincidence in the contact points. The height scale is 80 nm for height images, and the deflection scale is 10 nm for FV images. The image sizes are 0.5×0.5 μm.
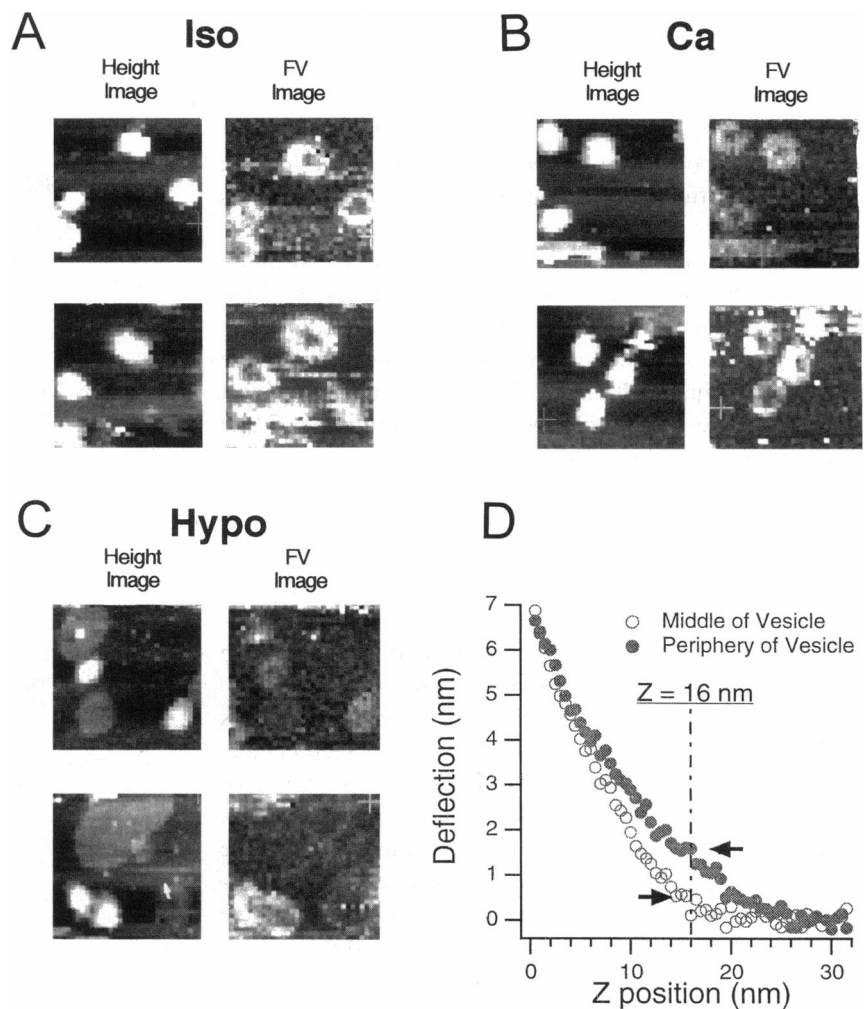
tions and are not an absolute measurement of any component of the vesicle. The AFM tip is not spherical on the atomic scale. At present there is no way to control or characterize the molecular roughness of the tip, and so we must assume that any roughness effects are negligible.

Second, the radii of the vesicles, as required for Eq. 4, are difficult to measure. Measured vesicle widths are not accurate because the lateral resolution is only ~15 nm/pixel and the effects of tip–sample convolution (Keller and Chih-Chung, 1991; Vesenka et al., 1993) are not known. Thus, the heights of the vesicles were used as an estimate of the vesicles' radii. The heights estimated here are less than those estimated by dynamic laser light scattering (Gracz and Parsons, 1996). This phenomenon may be due to partial flattening of vesicles because of interaction with the mica support. Any error in height will be relatively consistent, however.

Finally, the tip is on a cantilever that approaches the surface at an angle of 15° from horizontal. This means that the applied force has a small lateral component (Radmacher et al., 1994a). Although the lateral force may not be negligible, it is present in all the measurements, and so the effects were neglected.
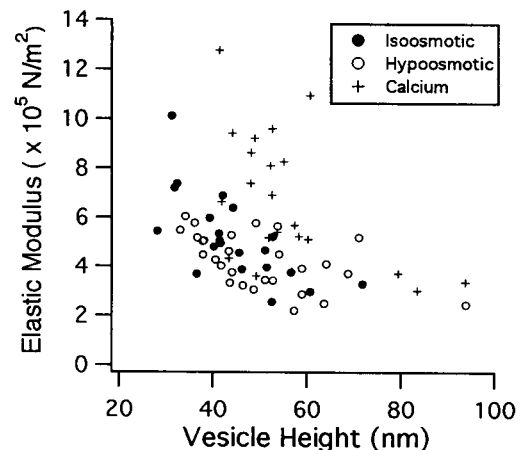
FIGURE 7   Scatter plot of elastic modulus versus height for the centers of vesicles in isoosmotic, hypoosmotic, and calcium buffers. The vesicle heights have been adjusted for indentation. The Wilcoxon rank-sum test was used to determine whether the populations are statistically different. For isoosmotic and hypoosmotic vesicles $p = 0.098$. Thus, there is no significant difference in Young's modulus. For isoosmotic and calcium buffers $p = 0.066$, and for hypoosmotic and calcium buffers $p < 0.003$. These values indicate that the elastic modulus is significantly higher for vesicles in calcium buffer than for vesicles in hypoosmotic buffer.

Buffer composition affects the elastic moduli of vesicular centers

The centers of vesicles in calcium buffer have a significantly larger mean elastic modulus than the centers of vesicles in hypoosmotic buffer. The centers of vesicles in isoosmotic buffer have an intermediate elastic modulus (Fig. 7).

Use of light scattering to measure hypoosmotic swelling has shown that Ca^{2+} decreases the elastic modulus of the chromaffin granule (Miyamoto and Fujime, 1988). Chromaffin granule membranes are similar to synaptic vesicle membranes. The results from chromaffin granules suggest that the vesicle membrane does not determine the elastic modulus measured by AFM.

The centers of vesicles have larger elastic moduli than the peripheries, as shown by the smaller indentations of the AFM tip at the centers. This suggests that an internal structure is the primary determinant of the hard centers of the vesicles in these experiments. The higher elastic modulus in calcium buffer is hypothesized to be due to the binding of calcium to an internal structure.

The hard centers seen in FV images of synaptic vesicles may correspond to the electron-dense particles seen in electron micrographs of synaptic vesicles in the presence of calcium-containing fixatives (Boyne et al., 1974; Mizuhira et al., 1994). Both electron microscopy and atomic force microscopy thus show evidence for a calcium-binding vesicular substructure or intravesicular component. All three buffers in the AFM experiments also have Mg^{2+}, which may bind to the same structure(s) as Ca^{2+} does.

The calcium-binding component in the centers of vesicles could be proteoglycan, which is located in the cores of vesicles (Walker et al., 1983). This core proteoglycan contains a sulfated glycosaminoglycan that can bind Ca^{2+} (Hunter et al., 1988; Scranton et al., 1993). The core glycosaminoglycan has been hypothesized to cross-link after exocytosis to prevent vesicle membrane proteins from diffusing laterally in the presynaptic membrane (Jones et al., 1982a,b). Ca^{2+}, which is ~ 1 mM in concentration in the synaptic cleft, may facilitate such cross-linking.

There also is evidence that synaptic vesicles sequester Ca^{2+} to keep the cytoplasmic Ca^{2+} concentrations low (Párducz and Dunant, 1993; Párducz et al., 1994). Vesicles can take up Ca^{2+} in vitro in the presence of ATP by means of a Ca^{2+}-ATPase (Rephaeli and Parsons, 1982; Párducz and Dunant, 1993). Vesicles may be able to take up Ca^{2+} passively in the presence of a favorable concentration gradient, as in these AFM experiments.

CONCLUSION

The AFM was able to detect hard centers in cholinergic synaptic vesicles and measured an increase in the elastic modulus when Ca^{2+} was present in the buffer.

REFERENCES

Boyne, A. F., T. P. Bohan, and T. H. Williams. 1974. Effects of calcium-containing fixation solutions on cholinergic synaptic vesicles. *J. Cell Biol.* 63:780–795.

Bustamante, C., and C. Rivetti. 1996. Visualizing protein-nucleic acid interactions on a large scale with the scanning force microscope. *Annu. Rev. Biophys. Biomol. Struct.* 25:395–429.

Calakos, N., and R. H. Scheller. 1996. Synaptic vesicle biogenesis, docking, and fusion: a molecular description. *Physiol. Rev.* 76:1–29.

Gracz, L. M., and S. M. Parsons. 1996. Purification of active synaptic vesicles from the electric organ of *Torpedo californica* and comparison to reserve vesicles. *Biochim. Biophys. Acta.* 2:293–302.

Hansma, H. G. 1996. Atomic force microscopy of biomolecules. *J. Vac. Sci. Technol. B.* 14:1390–1394.

Hansma, H. G., and J. H. Hoh. 1994. Biomolecular imaging with the atomic force microscope. *Annu. Rev. Biophys. Biomol. Struct.* 23: 115–139.

Hansma, H. G., D. E. Laney, M. Bezanilla, R. L. Sinsheimer, and P. K. Hansma. 1995. Applications for atomic force microscopy of DNA. *Biophys. J.* 68:1672–1677.

Henderson, E., P. G. Haydon, and D. S. Sakaguchi. 1992. Actin filament dynamics in living glial cells imaged by atomic force microscopy. *Science.* 257:1944–6.

Hunter, G. K., K. S. Wong, and J. J. Kim. 1988. Binding of calcium to glycosaminoglycans: an equilibrium dialysis study. *Arch. Biochem. Biophys.* 260:161–167.

Hutter, J. L., and J. Bechhoefer. 1993. Calibration of atomic-force microscope tips. *Rev. Sci. Instrum.* 64:1868–1873.

Jones, R. T., J. H. Walker, H. Stadler, and V. P. Whittaker. 1982a. Immunohistochemical localization of a synaptic-vesicle antigen in a cholinergic neuron under conditions of stimulation and rest. *Cell Tissue Res.* 223:117–126.

Jones, R. T., J. H. Walker, H. Stadler, and V. P. Whittaker. 1982b. Further evidence that glycosaminoglycan specific to cholinergic synaptic vesicles recycles during electrical stimulation of the electric organ of *Torpedo marmorata*. *Cell Tissue Res.* 224:685–688.

Keller, D., and C. Chih-Chung. 1991. Reconstruction of STM and AFM images distorted by finite-size tips. *Surf. Sci.* 253:353–364.

Lapin, L. L. 1975. Statistics: Meaning and Method. Harcourt Brace Javanovich, Inc., New York. 504–509.

Marx, J. 1996. Searching for drugs that combat Alzheimer's. *Science.* 273:50–53.

Miklossy, J., S. Kasas, R. C. Janzer, F. Ardizzoni, and H. V. d. Loos. 1994. Further ultrastructural evidence that spirochaetes may play a role in the aetiology of Alzheimer's disease. *Neuroreport.* 5:1201–1204.

Miyamoto, S., and S. Fujime. 1988. Regulation by Ca^{2+} of membrane elasticity of bovine chromaffin granules. *FEBS Lett.* 238:67–70.

Mizuhira, V., H. Hasegawa, and M. Notoya. 1994. Microwave fixation and localization of calcium in synaptic vesicles. *J. Neurosci. Meth.* 55: 125–136.

Noremberg, K., and S. M. Parsons. 1989. Regulation of the vesamicol receptor in cholinergic synaptic vesicles by acetylcholine and an endogenous factor. *J. Neurochem.* 52:913–920.

Párducz, A., and Y. Dunant. 1993. Transient increase of calcium in synaptic vesicles after stimulation. *Neuroscience.* 52:27–33.

Párducz, A., F. Loctin, E. Babel-Guérin, and Y. Dunant. 1994. Exoendocytotic activity during recovery from a brief tetanic stimulation: a role in calcium extrusion? *Neuroscience.* 62:93–103.

Parpura, V., R. T. Doyle, T. A. Basarsky, E. Henderson, and P. G. Haydon. 1995. Dynamic imaging of purified individual synaptic vesicles. *Neuroimage.* 2:3–7.

Radmacher, M., J. P. Cleveland, M. Fritz, H. G. Hansma, and P. K. Hansma. 1994a. Mapping interaction forces with the atomic force microscope. *Biophys. J.* 66:2159–2165.

Radmacher, M., M. Fritz, H. G. Hansma, and P. K. Hansma. 1994b. Direct observation of enzyme activity with the atomic force microscope. *Science.* 265:1577–1579.

Radmacher, M., M. Fritz, and P. K. Hansma. 1995. Imaging soft samples with the atomic force microscope: gelatin in water and propanol. *Biophys. J.* 69:264–270.

Radmacher, M., M. Fritz, C. M. Kacher, J. P. Cleveland, and P. K. Hansma. 1996. Measuring the viscoelastic properties of human platelets with the atomic force microscope. *Biophys. J.* 70:556–567.

Rephaeli, A., and S. M. Parsons. 1982. Calmodulin stimulation of transport and protein phosphorylation in cholinergic synaptic vesicles. *Proc. Natl. Acad. Sci. USA.* 79:5783–5787.

Schabert, F. A., C. Henn, and A. Engel. 1995. Native *Escherichia coli* OmpF porin surfaces probed by atomic force microscopy. *Science.* 268:92–94.

Schroff, S. G., D. R. Saner, and R. Lal. 1995. Dynamic micromechanical properties of cultured rat atrial myocytes measured by atomic force microscopy. *Am. J. Physiol.* 269:C286–C292.

Scranton, T. W., M. Iwanta, and S. S. Carlson. 1993. The SV2 protein of synaptic vesicles is a keratan sulfate proteoglycan. *J. Neurochem.* 61: 24–44.

Shao, Z., J. Mou, D. M. Czajkowsky, J. Yang, and J. Y. Yuan. 1996. Biological atomic force microscopy: what is achieved and what is needed. *Adv. Phys.* 45:1–86.

Tau, N. J., N. M. Lindsay, and S. Lees. 1992. Measuring the microelastic properties of biological materials. *Biophys. J.* 63:1165–1169.

Vesenka, J., S. Manne, R. Giberson, T. Marsh, and E. Henderson. 1993. Colloidal gold particles as an incompressible atomic force microscope imaging standard for assessing the compressibility of biomolecules. *Biophys. J.* 65:992–997.

Vinckier, A., C. Dumortier, Y. Engelborghs, and L. Hellemans. 1996. Dynamical and mechanical study of immobilized microtubules with atomic force microscopy. *J. Vac. Sci. Technol.* 14:1427–1431.

Walker, J. H., J. Obrocki, and C. W. Zimmermann. 1983. Identification of a proteoglycan antigen characteristic of cholinergic synaptic vesicles. *J.* Neurochem. 41:209–216.

Walters, D. A., J. P. Cleveland, N. H. Thompson, and P. K. Hansma. 1996. Short cantilevers for atomic force microscopy. *Rev. Sci. Instrum.* 67: 3583–3590.

Weisenhorn, A. L., M. Khorsandi, S. Kasas, V. Gotzos, and H.-J. Butt. 1993. Deformation and height anomaly of soft surfaces studied with the AFM. *Nanotechnology.* 4:106–113.

Young, W. C. 1989. Roark's Formulas for Stress and Strain. McGraw-Hill Book Co., New York.